Research Article | Vol. 10, No. 1 | 1 Jan 2019 | BIOMEDICAL OPTICS EXPRESS 50
Biomedical Optics EXPRESS

Megahertz-rate optical coherence tomography angiography improves the contrast of the choriocapillaris and choroid in human retinal imaging

JUSTIN V. MIGACZ,[1,*] IWONA GORCZYNSKA,[1,2] MEHDI AZIMIPOUR,[1] RAVI JONNAL,[1] ROBERT J. ZAWADZKI,[1] AND JOHN S. WERNER[1]

[1]*Vison Science and Advanced Retinal Imaging Laboratory, Department of Ophthalmology & Vision Science, University of California Davis, Sacramento, CA 95817, USA*
[2]*Institute of Physics, Faculty of Physics, Astronomy, and Informatics, Nicolaus Copernicus University in Torun, Grudziadzka 5, 87-100 Torun, Poland*
**jvmigacz@ucdavis.edu*

Abstract: Angiographic imaging of the human eye with optical coherence tomography (OCT) is becoming an increasingly important tool in the scientific investigation and clinical management of several blinding diseases, including age-related macular degeneration and diabetic retinopathy. We have observed that OCT angiography (OCTA) of the human choriocapillaris and choroid with a 1.64 MHz A-scan rate swept-source laser yields higher contrast images as compared to a slower rate system operating at 100 kHz. This result is unexpected because signal sensitivity is reduced when acquisition rates are increased, and the incident illumination power is kept constant. The contrast of angiography images generated by acquiring multiple sequential frames and calculating the variation caused by blood flow, however, appears to be improved significantly when lower-contrast images are taken more rapidly. To demonstrate that the acquisition rate plays a role in the quality improvement, we have imaged five healthy subjects with a narrow field of view (1.2 mm) OCTA imaging system using two separate swept-source lasers of different A-line rates and compared the results quantitatively using the radially-averaged power spectrum. The average improvement in the contrast is 23.0% (+/–7.6%). Although the underlying cause of this enhancement is not explicitly determined here, we speculate that the higher-speed system suppresses the noise contribution from eye motion in subjects and operates with an inter-scan time that better discriminates the flow velocities present in the choroid and choriocapillaris. Our result informs OCT system developers on the merits of ultrahigh-speed acquisition in functional imaging applications.

1. Introduction

Since its initial demonstration more than two decades ago [1], optical coherence tomography (OCT) has become a standard tool for visualizing the laminar structure of the retina. The rapid development of OCT performance has led to its widespread clinical adoption in ophthalmology and promising growth in dermatology and cardiology [2]. This continued growth and expansion is largely due to improvements in imaging speed, enabling the observation of faster dynamics in tissue and reduced motion artifacts [3]. One of the most exciting emerging applications of OCT is in the examination of retinal vasculature, widely seen as a way to observe a functional aspect of the visual system: the perfusion of blood. Though it has been recently termed OCT angiography (OCTA), research groups have been developing vascular imaging since the early years of OCT [4–6]. Currently, this capability is being transferred to the clinic through commercial development. With this increased

#346815 https://doi.org/10.1364/BOE.10.000050
Journal © 2019 Received 10 Oct 2018; revised 25 Nov 2018; accepted 27 Nov 2018; published 5 Dec 2018

Biomedical Optics EXPRESS

accessibility, several journal special issues, review articles, and international conferences now exist, highlighting studies done with both research and commercial OCTA systems [7–9].

The morphology of vasculature has important implications in some retinal diseases. The inner retinal vessels nourish the neural tissue other than the photoreceptors and retinal pigment epithelium. The choroidal vessels provide the significant amount of oxygen and nutrients that these outer two layers require and are a complex network of high-flow vasculature. Gross changes in retinal vasculature and large vessels of the choroid are clinically observable using fluorescein and indocyanine green angiography (FA and ICGA, respectively), and current OCTA methods offer a non-invasive alternative to these techniques that clinicians use to manage retinal disease. One of the most prevalent diseases that affects vision in a large fraction of the elderly is age-related macular degeneration (AMD). It is believed that defects of the choroid, particularly of the choriocapillaris layer, may play a significant role in the initial stages of the disease [10]. Detailed imaging of the choriocapillaris, therefore, may lead to a better understanding of the etiology and treatment of AMD.

Structural OCT images do not normally provide significant contrast between the retinal neurons and the vasculature. To detect the flow, an area of the retina is imaged multiple times in rapid succession to reveal the presence of moving scatterers, presumably blood cells moving in the vessels. OCT Doppler studies use phase changes to determine the velocity of objects traversing the imaging beam. In OCTA, the direction and velocity are ignored, and the brightness of the signal is determined by the variance of the OCT signal. Most angiography techniques do not quantify the blood velocity, but there is growing interest in quantifying flow in OCTA imagery, albeit imprecisely or in a relative sense [11–15]. Advancement towards these goals of better angiography have been marked by the utilization of progressively faster OCT systems.

A clear benefit of imaging with a rapid OCT acquisition system is that a wider region of the tissue can be captured within a conventional recording time [16,17]. Using a simultaneous 2-D retinal scanner, such as a scanning light ophthalmoscope, can track and correct eye motions artifacts and increase the achievable field of view of OCTA imaging [18–20]. As an alternative to capturing a larger area, one can record images of the same area more quickly, reducing the deleterious effect of object motion. Studies conducted with high-speed OCTA systems have shown that a rapid frame rate can significantly improve the visualization of the high-speed flows present in the choroid [21,22]. These results encouraged us to build an ultrahigh-speed system in which the B-scan frame rate is exceptionally fast, and many small-area images can be acquired in a similar timespan, yielding a much more temporally dense data set. Our main findings were that, despite the reduced signal sensitivity of such a high-speed system, the quality of choroidal and choriocapillaris images were unexpectedly good. Here, we demonstrate the improvement in image quality, which we believe is afforded by the rapid frame rate.

2. Design and methods

This study compares two OCT imaging systems of significantly different acquisition speeds by performing similar imaging on the same group of subjects. The optical systems were assembled from commercially-sourced components, and the acquired data were processed using software developed by the authors. The list of components, lens prescription, and post-processing scripts are included in the supplementary materials, which include Dataset 1, Dataset 2, and Dataset 3 [23–25]. In this section, we describe the general system, scan parameters, image processing, and image quality analysis.

The most significant component of our ultrahigh speed OCT system was the rapid wavelength-tuning laser source. It was a Fourier-domain mode-locked (FDML) laser (FDML-1060-750-4B-APC, OptoRes GmbH, Munich, Germany) operating at an A-scan rate of 1.644 MHz. The FDML device consists of a ring laser with a high-speed tunable filter within the

Biomedical Optics EXPRESS

loop and two buffering stages which create three replicates of the original wavelength-sweeping pulse group [26,27]. The other, slower, swept-source laser was also a commercial device (1060 nm SSOCT, Axsun Inc., Billerica, Massachusetts, USA) operating at a 100 kHz sweep rate, which is of a more similar speed to many OCTA systems in research groups and clinics. Table 1 lists the significant characteristics of the two OCT systems for comparison. The fiber couplers (OCT-060A42H10, Gooch & Housego Ltd, Torquay, Devon, UK) were connected in an arrangement such that the reference light is transmitted from one fiber tip to a second by way of a retroreflector on a sliding translation stage. Dispersion mismatch in the system is compensated using a small fiber patch cord, the length of which was determined by iteratively trying different cord lengths until the best correction was achieved. Any remaining dispersion mismatch was corrected numerically in post-processing. This two-couplers topology, diagramed in Fig. 1(A), allows for balanced detection, an essential feature when using swept-source lasers which have significant relative intensity noise [28]. The topology allowed the operator to easily adjust the reference power to maximize the sensitivity [29,30]. The exposure level of the imaging beam was set to 1.8 mW, below the limit determined by the ANSI standard for the safe use of lasers at this wavelength [31]. The measured sensitivity of the instrument was −95.3 dB when using the fast laser, and −107.4 dB for the slow one. The sensitivity was optimized by characterizing all the major noise sources and choosing the reference power level (3.2 mW on the photoreceiver) to ensure that the system was shot-noise limited. The phase noise was also measured for both systems by imaging both a mirror and paper sample near the zero-distance position, and the results are listed in Table 1. The signal-limited phase noise is the estimated by measuring the standard deviation of the noise in the OCT images, and dividing it by the magnitude of the OCT signal in the region of interest [21]. In this study, this region is the choriocapillaris layer, and the signal is averaged over all subjects.

Table 1. Summary of relevant acquisition parameters in the systems used.

System Parameters	Slower	Faster
Laser manufacturer	Axsun Inc.	OptoRes GmbH
Model number	1060 nm SSOCT	FDML-1060-750-4B-APC
A-scan rate	100 kHz	1.64 MHz
Center wavelength	1053 nm	1063 nm
Spectral bandwidth	100 nm	83 nm
Axial resolution in air (FWHM)	7.9 µm	9.6 µm
Optical beam size on pupil (FWHM)	1.09 mm	1.09 mm
Optical power at cornea	1.8 mW	1.8 mW
Measured sensitivity	−107.4 dB	−95.3 dB
System phase noise (RMS)†	66 mrad	2.6 mrad
Signal-limited phase noise (RMS)*	31.9 mrad	133.3 mrad
Horizontal field of view on retina‡	1.2 mm	1.2 mm
Vertical field of view on retina‡	0.46 mm	1.2 mm
Number of A-scans per B-scan	400	392
Number of vertical positions in volume	180	392
B-scan rate	200 Hz	1.99 kHz
Number of repeated B-scans	5	10
Volume scan time	4.50 sec.	1.96 sec.

† Phase noise calculated with the bulk-phase correction applied to the image sequence.
* Theoretical phase noise value determined by the ratio of the image noise over the signal value in an area of interest, which is the choriocapillaris layer in this case [21].
‡Based on an assumed 16.67 mm effective focal length of the human eye.

The sample arm was assembled from commercially available lenses, scanners, and optomechanics. The first lens after the fiber output was a 0.5 inch diameter achromat with a focal length of 18 mm. For the fast system, the first scanner in the beam path was a galvanometer scanner (8310KM40B, Cambridge Technologies Inc., Bedford, MA, USA) which scanned the beam vertically. The nearby (7 mm away) second mirror was a resonant scanner (SC-30, Electro-Optical Products Corp., Ridgewood, NY, USA) oscillating at 1.994

Biomedical Optics EXPRESS

kHz. This rate allowed for 430 A-scans during both forward and backward scans separately. Only the center 392 A-scans of each were kept for later processing. When using the slower laser, the 100 kHz swept-source, a galvanometer scanner (6210HSM40, Cambridge Technologies Inc.) was substituted in the place of the resonant scanner. The optical layout between the scanners and the subject's eye was a 2f-2f imaging system. In this arrangement, the objective lens, composed of two achromatic lenses, was approximately two focal lengths away from the scanners so that their conjugate image was approximately two focal lengths in front of the objective. The objective's focal length was ~38 mm. Defocus of the beam was adjusted by displacing the fiber tip axially. This design was used for its relative compactness and to reduce the number of optical surfaces.

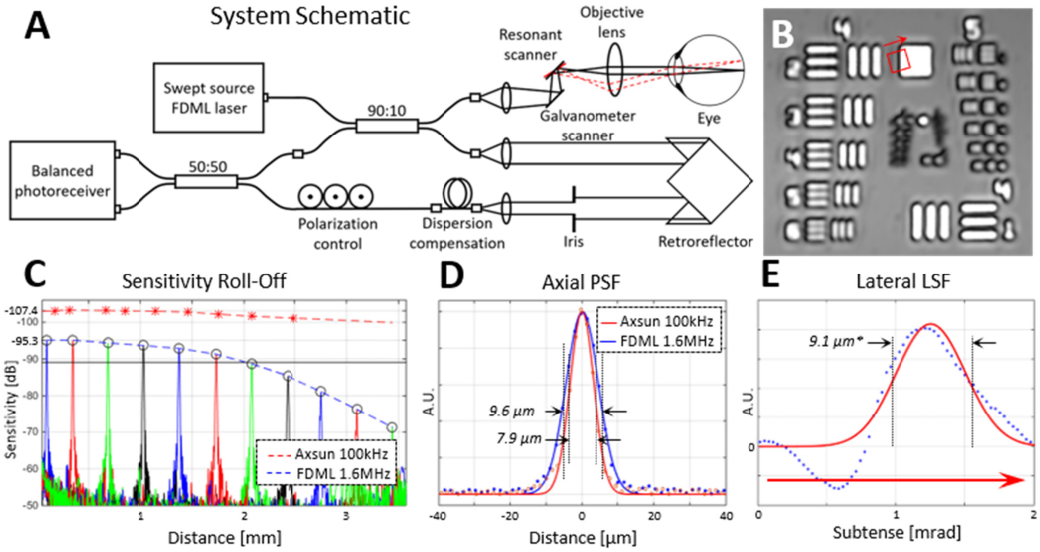

Fig. 1. Specifications of the imaging system. (A) Optical system layout using two fiber couplers to enable balanced detection. A small, custom fiber patch cord is added to the reference portion of the interferometer to compensate for most of the dispersion mismatch. (B) Image of a 1951 USAF resolution test chart imaged through a 50 mm lens in the place of the subject's eye. Elements from group 4 and the first from group 5 are clearly visible. (C) Sensitivity roll-off graph of the systems is shown as determined with a calibrated mirror. Sensitivity is reduced to 6 dB below the peak value at approximately 2 mm of distance in the fast FDML system. For the slower system, the –6 dB point is beyond the ~3.5 mm range of the acquisition. (D) The axial resolution of the two systems. (E) Lateral line-spread function, measured as an angular subtense, is a proxy for the lateral point-spread function. It was determined from a fit (red curve) of the derivative (blue dots) of the feature edge highlighted by the red square and arrow in (B). The resolution (9.1µm) denoted in E indicates an indirect estimation of the angular resolution multiplied by the effective focal length of a standard human eye (16.7mm).

The five subjects recruited for this study were provided written informed consent, in accordance with a protocol approved by the Institutional Review Board of the University of California at Davis. They had no known pathologies in the eyes that were imaged. The summary of the subject information is provided in Table 2. Subjects were aligned to the imaging system using a bitebar and forehead rest. Between 9 and 18 retinal locations were imaged within the macula. Each location was imaged twice. Random eye drift and saccades result in small sections of the target area to be missed or distorted. Repeated measurements, therefore, increased the possibility that most tissue within the targeted area would have been captured.

Biomedical Optics EXPRESS

Table 2. Details about the 5 subjects without ocular pathology used in this study.

	Subject 1	Subject 2	Subject 3	Subject 4	Subject 5
Gender	Male	Female	Male	Male	Female
Age	32	41	45	36	20
Eye imaged	Right	Right	Right	Left	Right
Spherical refractive error	+ 2.5 D	0 D	+ 3.0 D	0 D	+ 0.25 D

Generating an angiographic image requires that motion of the blood cells within the vasculature be detected. As in most OCTA methods, sequential B-scans were acquired at the same position multiple times such that temporal changes in the cross-section could be captured. In both systems the fast and slow scanning directions were the horizontal and vertical directions, respectively. For the fast system (~1.64 MHz), which operated with an approximately 2 kHz B-scan rate, scans were repeated at every vertical position 10 times before moving to the next position. A total of 392 separate vertical positions were captured in each volume, which amounted to 3920 total B-scans. This resulted in a volume acquisition time of 1.96 seconds. For the slow system (100 kHz), which had a B-scan rate of 200 Hz, only 5 repetitions were performed at each position, and 180 vertical positions were collected for a total of 900 B-scans in every volume. If the slower system were configured to acquire the same number of B-scans as the faster system, and over the same field of view, the time required would be 19.6 seconds. This duration is not practical in most human retinal imaging because of the relatively short drying time of the tear film, the consequent blinks and loss of fixation.

The scanning range for images taken with the fast system was 4°x4° for the fast system and 4°x1.6° for the slow one, which corresponds to approximately 1.2x1.2 mm and 1.2x0.55 mm on the retina, respectively. The resonant scanner of the fast system has sinusoidal distortion which is corrected after the intensity and angiogram images are processed. To determine the appropriate interpolation, a grid-pattern test target was imaged and analyzed every few months. The average pixel pitch of both systems was approximately 3.1 μm. These sampling densities are approximately 3 times smaller than the full-width at half-maximum (FWHM) spot size diameter which was estimated to be 9.1 μm from the line-spread function shown in Fig. 1(E), and most OCTA studies do not exploit oversampling to such a degree [17].

The acquired data were post-processed in separate software to generate the vascular maps of the tissue. The angiography method used here is the phase-variance method, which computes the variance of the phase component of each pixel [32–35]. The unwanted effect of bulk motion of the tissue is compensated using the method described by Makita et al. [32]. The magnitude value of each pixel was not considered except in computing a threshold on the image. This threshold determined which phase pixels would be used in the final angiogram. We have found that adjusting the threshold value can have a significant impact on the appearance of the vascular network that the user chooses to target. In all images taken for both systems, the threshold was chosen iteratively by the user to best elucidate the vasculature of interest. Angiogram volumes were then flattened with respect to the vascular bed of interest to create *en face* representations of vascular networks. We used the graph-cut method to segment the retinal pigment epithelium (RPE) in each image and flatten the volume according to the segmented trace [36].

We quantified the image quality of the choriocapillaris vessels by using the radial average of the spatial 2-D discrete Fourier transform (DFT). We refer to this as the radially-averaged power spectrum (RAPS) curve, although one could similarly call it a concentrically-averaged power spectrum. RAPS curves were presented in a logarithmic magnitude scale. Because most images had differing brightness ranges, the RAPS curves were normalized by pinning the maximum and minimum values between unity and zero. These curves allowed us to examine the contrast of the spatial frequencies present in the image. Other studies have used

Biomedical Optics EXPRESS

RAPS curves in similar ways to identify the predominant feature density in retinal cone images [37,38] and choriocapillaris vessel spacing [39,40].

3. Results

Our initial observation was that angiograms of the choroicapillaris produced using the high-speed (1.64 MHz) FDML laser are qualitatively better than those produced by a slower (100 kHz) swept laser. This was unexpected because the signal of a fast A-scan is generated with ~1/16 of the collected photons and has a consequently lower signal-to-noise ratio (SNR).

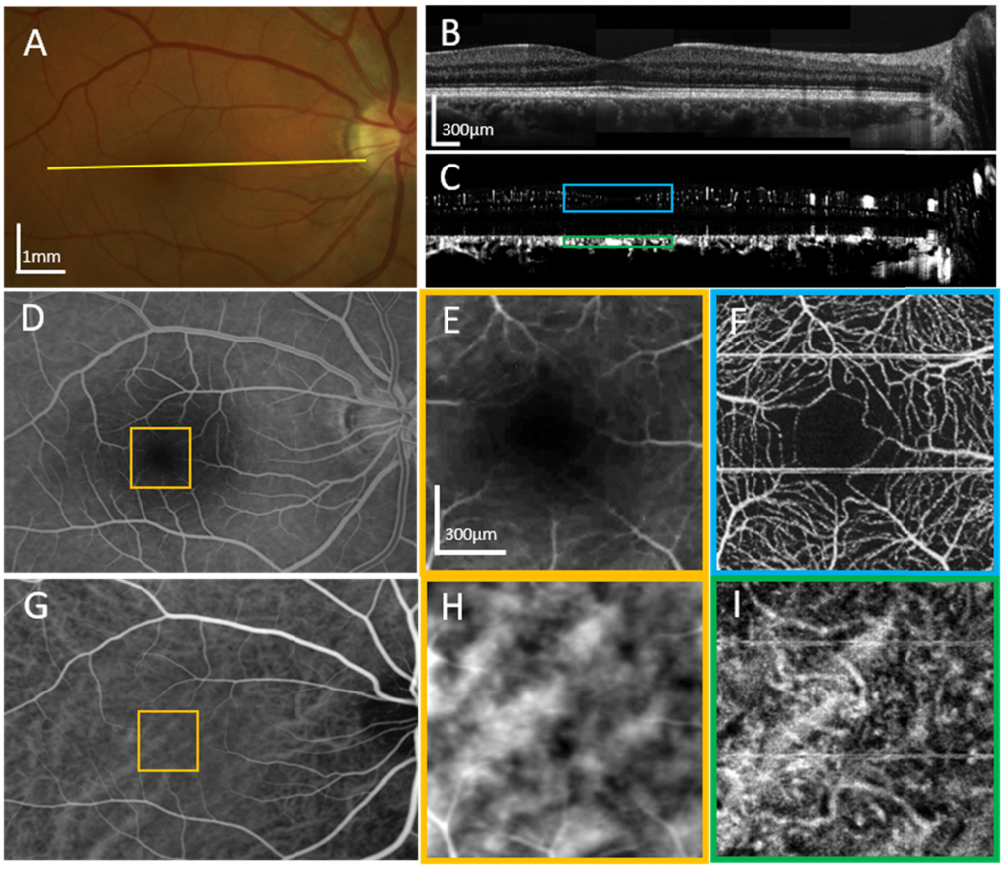

Fig. 2. A comparison of standard clinical imaging and our high-speed OCTA imaging of the right eye of subject 1, a 32-year-old male, without known ocular pathology. (A) A color fundus photo in which some of the large vessels are visible. (B) A mosaic of 8 adjacent OCT B-scans taken with the FDML system. (C) OCTA images from the same data as (B). The locations for both (B) and (C) are indicated by the yellow line in (A). (D) A fluorescein angiogram of the same eye reveals finer retinal vasculature than the fundus photo. (E) A zoomed-in section of the fluorescein angiogram centered at the fovea. (F) An OCTA projection of the same area from (E) shows a much more detailed view of the vessels including the capillaries. (G) An indocyanine green angiography (ICGA) image shows some of the larger choroidal vessels more clearly, owing to the near-infrared fluorescent emission scattering less in the pigment epithelial cells than the visible emission of (D). (H) A zoomed-in section of the ICGA scan. (I) An OCTA projection of the same area as in (H) reveals more detail of the choroidal vessels. Both (E) and (H) have had their brightness and contrast adjusted to highlight details in the narrow region. The blue and green squares in (C) show the depth ranges that were integrated to generate the images in (F) and (I), respectively.

As a first qualitative comparison, we acquired images of the retinal and choroidal vasculature of one of our subjects using color fundus photography (FP), fluorescein

Biomedical Optics EXPRESS

angiography (FA) and indocyanine green angiography (ICGA), which are all standard modalities for clinicians. The examples of the clinical images, alongside the high-speed OCTA images are shown in Fig. 2. The clinical images are shown in panels 2-A, D, E, G, and H, and high-speed OCT/OCTA images (2-B, C, F, I) of subject 1, a 32-year old male with no known ocular pathology. Together, the images provide an overview of the angiographic capabilities of the high-speed FDML system. Large vessels are visible in the fundus photo (2-A). Images of OCT intensity (2-B) and OCT angiography (2-C) were generated by averaging and computing phase variance, respectively, on 10 repeated scans. The B-scans were acquired at the location indicated by the yellow line in the fundus photo (2-A). The stitched B-scan images are composed of 8 laterally overlapping narrow-field scans spaced about 1 mm apart on the retina. The cross-sectional intensity image reveals detail comparable to that of a commercial SD-OCT system, and the corresponding angiogram reveals vascular detail at all layers in the retina. A fluorescein angiogram (2-D) shows retinal vasculature, while a comparison between its foveal region (2-E) and the corresponding high-speed OCTA region (2-F) reveals the latter to show much better detail. An indocyanine green angiography image (2-G) shows some of the larger choroidal vessels, but a comparison between its magnified foveal region (2-H) and the corresponding OCTA image (2-I) demonstrates the significantly finer detail revealed by high-speed OCTA. Panels (2-E) and (2-H) have had their brightness and contrast adjusted to highlight the details in the narrow region. The blue and green squares in (2-C) show the depth ranges that were integrated to generate the images in (2-F) and (2-I), respectively.

While the OCT angiograms computed from low-speed images revealed significant detail in retinal and choroidal vascular layers, increasing B-scan rate improved the apparent contrast. Figure 3 shows a direct comparison of angiograms taken with the slow (100 kHz) and fast (1.64 MHz) systems, shown in the left and right halves of the figure, respectively. These images were centered on the fovea of subject 4, a 36-year-old emmetropic male. Cross-sectional intensity images (3-A and C) show similar details. Cross-sectional angiograms (3-B and D) reveal the retinal vasculature and choroidal vasculature. White arrows in the angiogram B-scans (3-B and D) indicate the outer retinal bands, where angiographic signal is not expected or at least minimal. Spurious signal, presumably due to bulk motion and indicated by the white arrows in the images, is visible in the low-speed (3-B) but noticeably more suppressed in the high-speed (3-D) angiogram. *En face* projections of the retinal vasculature (3-E and F) demonstrate that the high-speed has similar detail to the low-speed image. White arrowheads in those panels indicate that a small branch which appears fainter in the fast system image. In another scan taken moments later (not shown), the same segment is of similar brightness to nearby vessels. This suggests that a temporary flow reduction occurred during the initial scan. *En face* projections of the choriocapillaris (3-G and H) demonstrate the improved contrast and detail achieved by the high-speed system. While many superficial similarities are present between the images, the high-speed angiogram reveals a detailed, continuous meshwork of vessels not apparent in most of the low-speed image. In the deeper choroid, the low-speed angiogram (I) is slightly noisier than the high-speed angiogram (J), and the latter reveals better small vessel detail and improved visibility of vessel continuity, though details of the choroid are clearly apparent in both.

Biomedical Optics EXPRESS

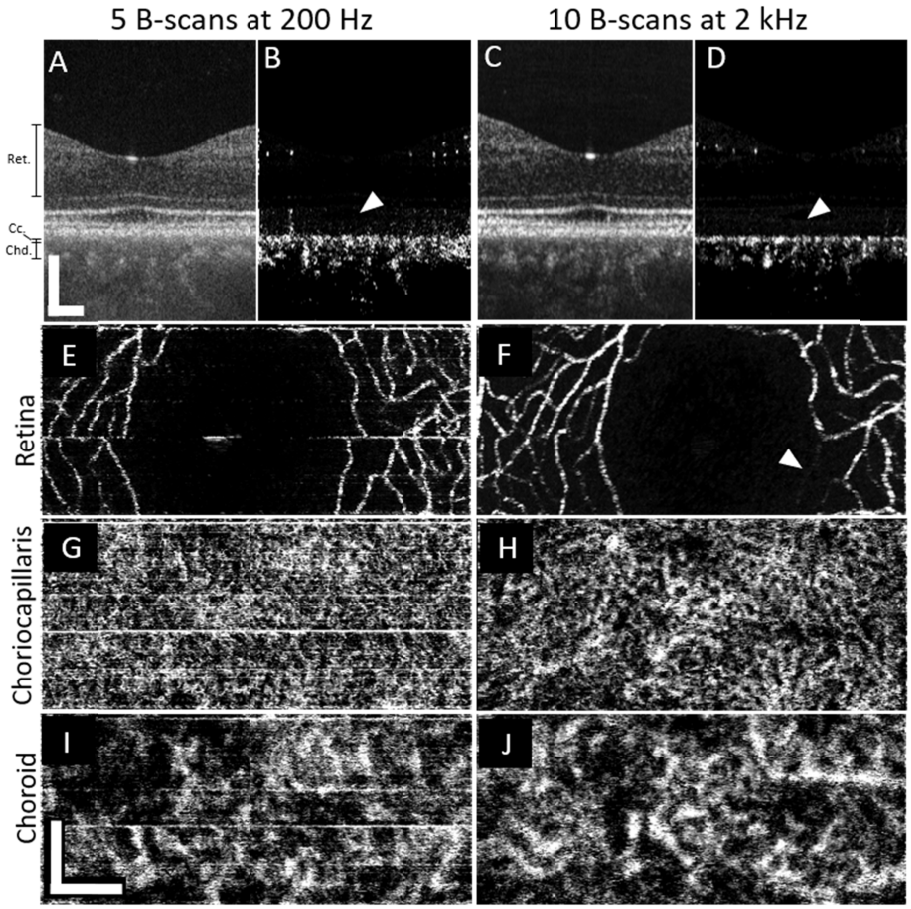

Fig. 3. A direct comparison of the imaging performance of the two swept-source systems of a foveal scan from subject 4, a 36-year-old emmetropic male. Images from the slow system are shown on the left half (A,B,E,G,I) of the figure while the right half (C,D,F,H,J) shows images produced using the fast system. *En face* images from the fast system (right side) have been cropped, height-wise, to match the corresponding images from the slower system (left side). White arrows in B and D show that the fast system suppresses bulk motion-related noise in the vessel-free region of the pigment epithelium and photoreceptors better than the slow system. A white arrowhead in F shows that in a specific retinal capillary appears fainter in the fast system, most likely due to a momentary reduction of flow during the short period of scanning. All scale bars are 200μm.

While the benefits of higher speed are qualitatively apparent in the comparisons shown in Fig. 3, we sought to demonstrate these benefits quantitatively as well. Figure 4 gives an example of a radially-averaged power spectrum (RAPS), which can be used to quantitatively evaluate an image. Projections of choriocapillaris from the slow and fast systems were generated (left panels), and the two-dimensional discrete Fourier transformations (DFT) were computed (center column). In both DFTs, rings corresponding to the choriocapillaris network are visible. Because the choriocapillaris is a dense, and somewhat regularly-spaced network of vessels, a concentration of energy at a consistent radial range in the power spectrum is expected. Radial averaging of the log power spectra (right panels) permits a comparison of the contrasts. In the frequency of interest (26 cycles/mm), the contrast of the high-speed angiogram was 35% higher than that of the low-speed angiogram for these two images alone.

Biomedical Optics EXPRESS

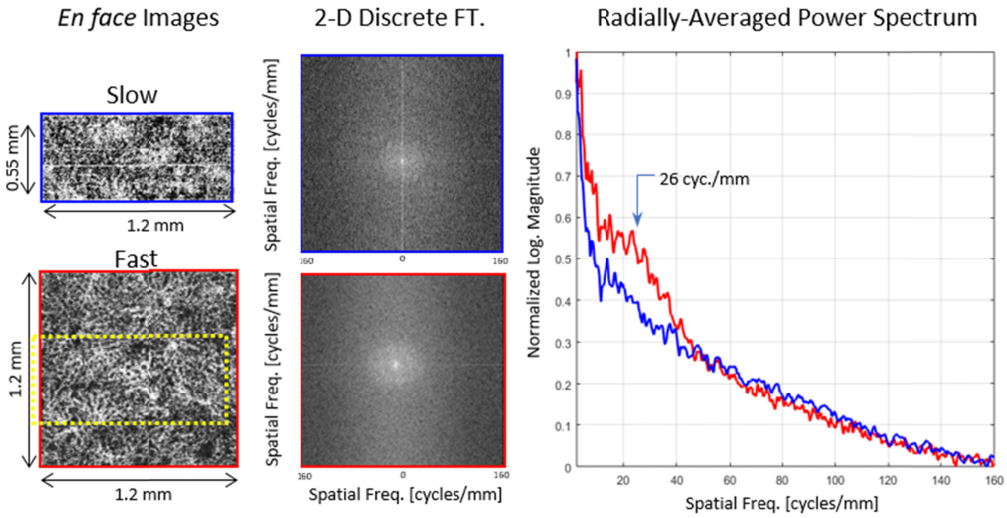

Fig. 4. Example of radially-averaged power spectra for two images taken at the foveal center on subject 4. The left column shows the two original *en face* projections of the choriocapillaris using the slow (top) and fast (bottom) systems. The dashed yellow rectangle in the bottom-left image indicates where the top-left image is located relatively. The 2D discrete Fourier transform of both images is shown in the middle column. From each point in the 2D spectral image, the radial distance is computed and summed into the appropriate frequency bin of the point in the plot to the right. The maxima and minima of each curve are set to the boundaries of one and zero, respectively.

RAPS curves were computed for all five subjects. To reduce noise in the power spectra, RAPS curves from multiple (9-18) locations in the macula were averaged. Plotted results from the five subjects are shown in Fig. 5. In each subject, three RAPS curves were computed, using 10 repeats of the high-speed system (red), 5 repeats of the high-speed system (green), and 5 repeats of the low-speed system (blue). In the fast system, 5-repeat protocol, only the first 5 of the 10 scans were used to compute the angiogram. For all three approaches in all five subjects, "knees" or bumps were visible at approximately 26-37 cyc./mm, depending on the subject.

The height of the knee in each RAPS curve is a measure of the contrast of the image at the given spatial frequency which is most likely caused by the somewhat regular vessels of the choriocapillaris. This position in the power spectrum thus serves as a basic metric for choriocapillaris image quality. The bar plot (lower right panel) shows the choriocapillaris contrast for each subject. In all subjects, the high-speed, 10-repeat protocol (red) produced the highest contrast, an average of 23.0% (+/– 7.6%) above that of the slow system (blue). The 5-repeat protocol (green) produced an average improvement of 7.48% (+/– 4.3%). In all subjects, even the high-speed 5-repeat protocol produced higher contrast than the low-speed 5-repeat protocol. The error bars in the bar graph show the standard deviation of the RAPS magnitude at the frequency of interest from the subject's macular images. It is evident from these RAPS curves that noticeable variation in choriocapillaris density exists among subjects, with the density of subject 1 (37 cyc./mm) significantly higher than that of the other subjects.

Biomedical Optics EXPRESS

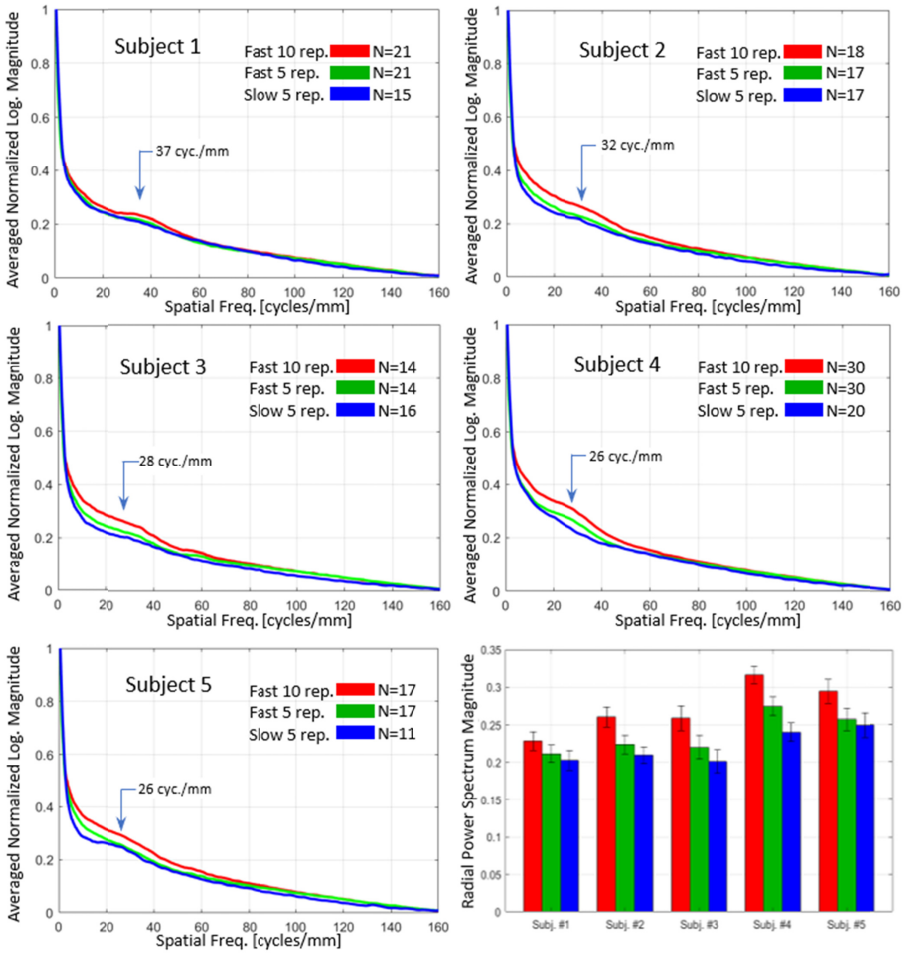

Fig. 5. Radially-averaged power spectrum (RAPS) curves of the choriocapillaris images from all five subjects (top left, top right, middle row, and bottom left). All curves are the averages from many individual images taken throughout the macula, as designated by the number (N) in the legend of each panel of the figure. A summary bar chart of the relative heights of the power spectrum at a chosen spatial frequency is shown in the bottom right. The chosen frequency roughly matches the density of choriocapillaris vessels and the knee shape in the curve. Error bars denote one standard deviation.

As a demonstration of the utility of the angiographic imaging of the fast system we have constructed three angiogram montages at different depth sections, shown in Figs. 6 and 7. The images were acquired in the macular regions of subjects 1 and 4. Each mosaic consists of 15 and 18 angiograms, respectively, manually aligned without intra-volume motion correction. A maximum intensity projection of the neural retina (top panels) shows the retinal vasculature. Stitching together the mean choriocapillaris projections reveals a dense network of small vessels across the entirety of the macula (center panel). As described above, subject 1 had the highest choriocapillaris spatial frequency (37 cyc/mm). Despite this, vessels are resolved everywhere, even in the foveal center, which has not been observed in slower OCTA systems except when utilizing adaptive optics [39]. Mean projections of the upper choroid (bottom panel) show a complex network of well-resolved vessels with a variety of apparent diameters in both subjects. In subject 4 (Fig. 7), multiple small regions void of choriocapillaris vessels are seen within the mosaic.

Biomedical Optics EXPRESS

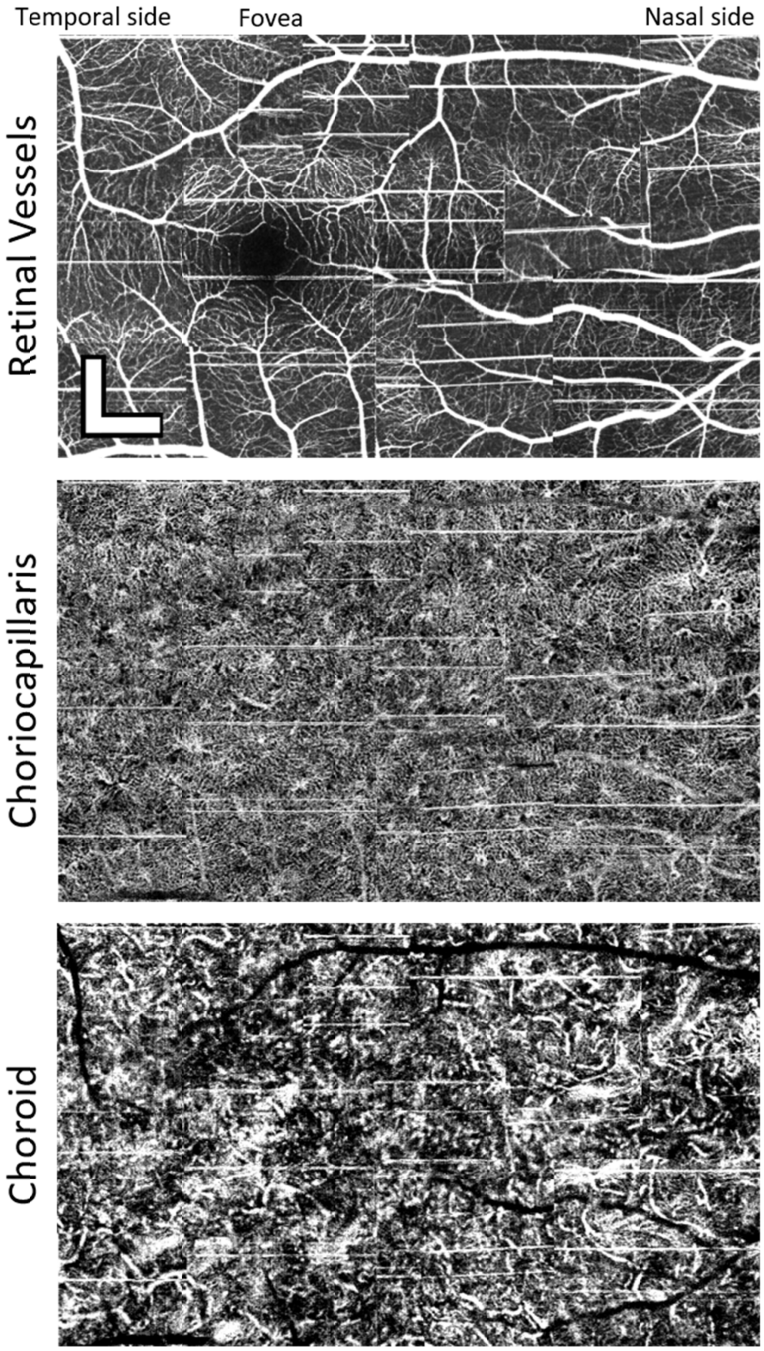

Fig. 6. Example of a mosaic of 15 images taken from the right eye of Subject 1, a 32-year-old male with 2.5 diopters of myopia. The images were taken with the high-speed system. The first mosaic shows the maximum intensity projection of all the outer retinal layers. The second panel shows a mean of the projections within the range of the choriocapillaris. The bottom mosaic shows a mean projection of the choroid. Depth ranges of each projection are the same as those indicated by the annotations to the left of Fig. 4(A). Images are stitched together manually without any intra-volume motion correction. Scalebars are 300μm.

Biomedical Optics EXPRESS

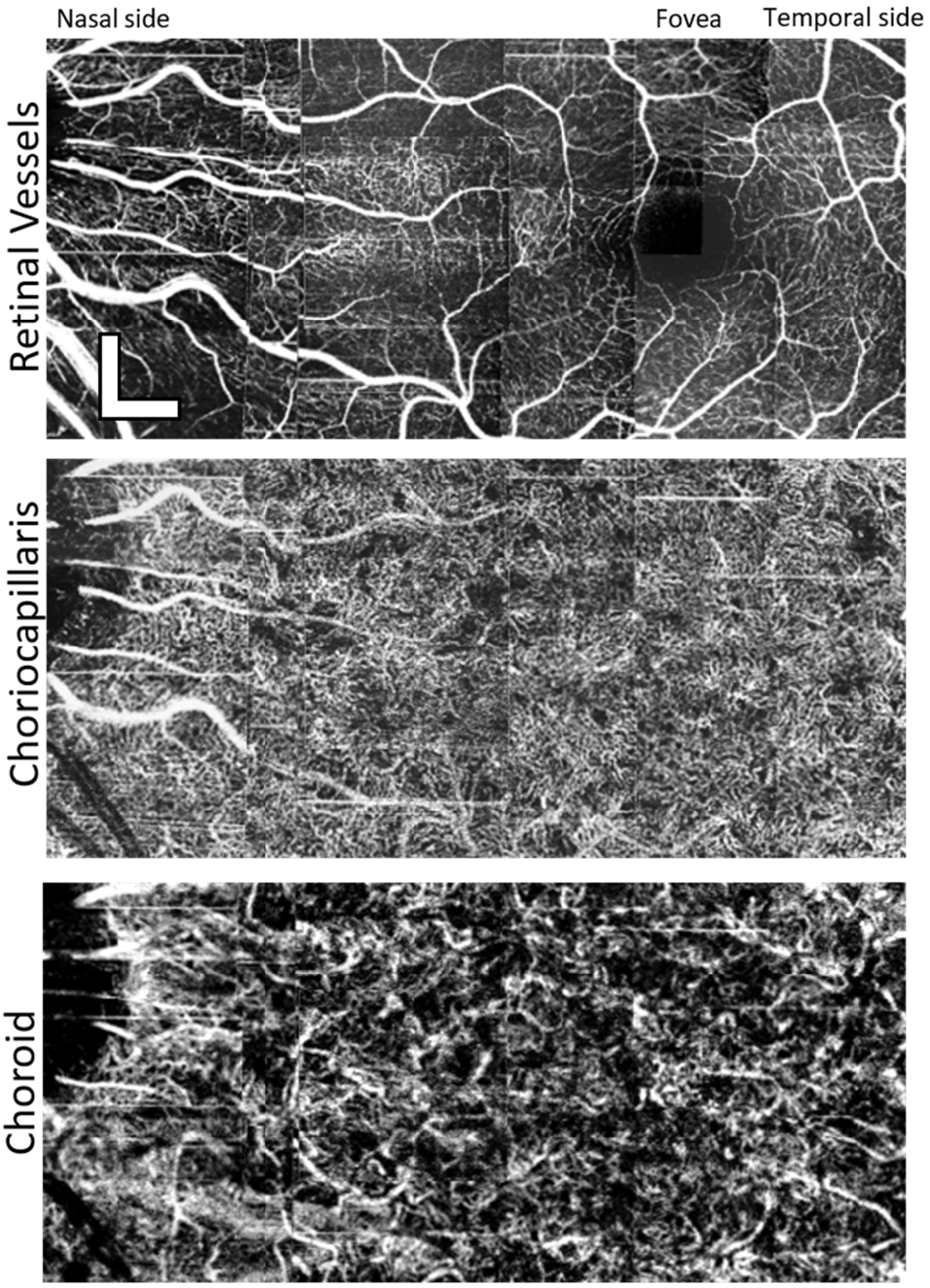

Fig. 7. Example of a mosaic of 18 images taken from the left eye of Subject 4, a 36-year-old emmetropic male. The images were taken with the high-speed, 1.64 MHz system. The images were assembled in the same manner as for Fig. 6. It is noteworthy that the choriocapillaris appears so have different vessel densities between the two subjects. Scalebars are 300μm.

4. Discussion

The most significant finding from this study is that despite the inherent loss of sensitivity from increased acquisition speed, imaging blood motion is improved. We must qualify this

Biomedical Optics EXPRESS

statement in that it is probably only true within a range of flow speeds and signal magnitudes. Our success here was partly serendipitous and partly the result of designing the system for specifically defined goals. It was clear from earlier work by Choi et al. and Braaf et al. that high-quality images of the choriocapillaris and choroid were possible with a high frame speed [14,21,22]. Based on the findings from these studies, we chose the B-scan rate and repetition number of our system to be optimized for imaging this vascular bed. In Choi's work, high-quality images of the choriocapillaris were generated with a 400 kHz system. The analogous images taken with our system, whose A-scan speed is about 4 times faster and B-scan speed is about 5 times faster, reveal the choriocapillaris morphology more clearly. The choriocapillaris in our images is even well defined in and around the fovea. There may be many differences between our system and theirs, but the most obvious one is the speed. In general, the parameters that predominantly affect OCTA images are the sensitivity, phase noise, B-scan repetition number, pixel pitch (sampling density), and inter-scan time, and we discuss these below. This study supports our belief that the inter-scan time has the most substantial effect on image quality enhancement.

The fringe amplitude sensitivities of the two systems are predictably different. The fast system was measured to have approximately −95 dB, and the slow system to have −107 dB. The fringe phase noise was measured to be lower in the fast system, but phase noise, by itself, cannot account for the improvement of the images. Even though the characterized phase noise of the slower system's laser is higher than that of the faster laser and higher than the signal-limited phase noise (see Table 1), it is our observation that this is not a limiting factor when imaging subjects. Those with exceptional fixation still generate a larger background signal due to movement than a stationary scattering object of similar signal level. It should also be noted that if a lower phase noise was the reason for the improvement, then spectrometer-based OCT systems, which are inherently very phase-stable, would be highly superior to swept-source ones for angiographic imaging. That does not appear to be the case, given the multitude of successful OCTA studies which have not revealed choriocapillaris and choroid images of high contrast. In many of these systems, the algorithms used ignore the phase information altogether.

As for the matter of repeated scans, the fast system captured many more frames within the usual OCT scan duration. It acquired B-scans at a 2 kHz frame rate and captured two mirrored B-scans during the front and back sweeps of the resonant scanner, which are then averaged after the angiogram is generated. Also, the chosen repetition number, 10, is twice as large as that used for the slower system. Both these measures might, at best, render two doublings of SNR. That four-fold improvement, however, does not overcome the theoretical sensitivity advantage of the slower system, which is 16 times (+ 12 dB) that of the fast system. The actual, quantifiable improvement is somewhat unclear and depends on how noise affects the discrete steps of the angiography post-processing method. The method used here is termed the phase variance algorithm, but specifics about how this algorithm theoretically compares to the multitude of others used in the field are not discussed here. We have previously reported an empirical comparison, however [41]. Most relevant is that the slower system should have a signal quality advantage, but it is outperformed by a fast system which scans the same area in much less time.

The sampling densities for both systems are unusually high when compared to those used in other studies. We have sampled at 3 times the density of the point spread function's full-width at half-maximum, which many would consider to be unnecessarily dense. Sampling density does make a difference in the appearance of OCTA angiograms, and previous work by our group has briefly explored this idea [17,40]. The angiograms of the slow system are still better than most reported in the literature with systems of similar speeds, possibly improved by the slightly smaller focused spot size as well. Because these parameters are consistent between the two systems, the main finding, that the fast system generates better images, still holds.

Biomedical Optics EXPRESS

The variables in this experiment have been controlled such that the main difference between the two systems is the inter-scan time. The slow system has about 5 ms between subsequent frames, while the fast system has 0.5 milliseconds between them. The effect of scatterer speed and inter-scan time has been explored in controlled flow-phantom experiments [11,12] and *in vivo* angiography images [14,15,21]. These studies have all demonstrated that the relative flow speed of blood can be inferred from the magnitude of the angiography signal, but the quantitative flow velocity cannot be determined accurately. When flow speeds are high or, equivalently, the inter-scan time is large, the speckle or phase image is maximally decorrelated, and the variance is essentially saturated in magnitude of the OCTA signal. This leads to any local variations of the flow speeds to become indistinguishable and so the vessel image is distorted and somewhat obscured. At the other extreme, when the flow speeds are low, or the interscan time is very short, the magnitude of flow-dependent changes become comparable to and indistinct from the background noise. The processes that contribute to angiography signal and the noise, however, may have different temporal frequency characteristics. The background noise is generally spectrally flat, so it contributes to a wideband noise floor in the temporal spectrum. Patient motion creates some low-frequency variation of the image, but much of that is suppressed by acquiring the frames rapidly, and bulk phase correction. The blood flow, the signal of interest, is probably somewhat band-limited, assuming we take the samples quickly. Taking many fast samples can help distinguish the signal from the acquisition noise, and motion. This strategy lessens the chance that some of its temporal variance (the sum of all the AC frequency bins) will be aliased into the stationary (the DC) frequency bin of the temporal discrete Fourier transform (DFT), resulting in some minor improvement in OCTA signal which is derived from the AC frequencies of the DFT. While we have demonstrated that increasing acquisition speed improved angiogram quality, we have not concluded that further increases in speed will result in corresponding image quality gains. At some very high speed and correspondingly low sensitivity, flow-dependent variation in the complex signal will fall below the noise floor, and the angiographic signal will be too low to be useable. An ideal frame-rate and dwell time should, we expect, exist for every flow speed range and scatterer signal strength. For imaging the choroid and choriocapillaris, as well as the inner retinal vessels, our chosen frame rate and repetition number worked well.

5. Conclusions

This study demonstrated that *in vivo* OCTA imaging of the choriocapillaris and other retinal vasculatures is significantly improved by using an ultrahigh-speed system with a 1.64 MHz A-scan rate. By comparing two similar OCTA systems that had different acquisition speeds, it appears that the critical advantage of the higher-speed system was the short inter-scan time and ability to take a multitude of repeated scans. This result should have a significant impact on how OCT system developers choose to operate their systems for imaging vasculature in the living eye.

Funding

National Eye Institute (NEI) (R01 EY024239, P30 EY012576, T32 EY15387).

Acknowledgments

We gratefully acknowledge the contributions of Susan Garcia of the VSRI Lab, for helping perform the OCTA and standard clinical imaging on all of our subjects. We thank Drs. Thomas Klein and Wolfgang Weiser from OptoRes GmbH for their extensive help with installing the FDML laser and providing acquisition software. We would also like to thank Dr. Yifan Jian, from Simon Fraser University, for providing the acquisition software for our 100 kHz SSOCT system.

Biomedical Optics EXPRESS

Disclosures

The authors declare that there are no conflicts of interest related to this article.

References

1. D. Huang, E. A. Swanson, C. P. Lin, J. S. Schuman, W. G. Stinson, W. Chang, M. R. Hee, T. Flotte, K. Gregory, C. A. Puliafito, and J. G. Fujimoto, "Optical coherence tomography," Science **254**(5035), 1178–1181 (1991).
2. J. Fujimoto and E. Swanson, "The development, commercialization, and impact of optical coherence tomography," Invest. Ophthalmol. Vis. Sci. **57**(9), OCT1–OCT13 (2016).
3. J. F. de Boer, R. Leitgeb, and M. Wojtkowski, "Twenty-five years of optical coherence tomography: the paradigm shift in sensitivity and speed provided by Fourier domain OCT [Invited]," Biomed. Opt. Express **8**(7), 3248–3280 (2017).
4. Z. Chen, T. E. Milner, D. Dave, and J. S. Nelson, "Optical Doppler tomographic imaging of fluid flow velocity in highly scattering media," Opt. Lett. **22**(1), 64–66 (1997).
5. Z. Chen, T. E. Milner, S. Srinivas, X. Wang, A. Malekafzali, M. J. C. van Gemert, and J. S. Nelson, "Noninvasive imaging of in vivo blood flow velocity using optical Doppler tomography," Opt. Lett. **22**(14), 1119–1121 (1997).
6. J. A. Izatt, M. D. Kulkarni, S. Yazdanfar, J. K. Barton, and A. J. Welch, "In vivo bidirectional color Doppler flow imaging of picoliter blood volumes using optical coherence tomography," Opt. Lett. **22**(18), 1439–1441 (1997).
7. R. F. Spaide, J. G. Fujimoto, and N. K. Waheed, "Optical coherence tomography angiography," Retina **35**(11), 2161–2162 (2015).
8. S. S. Gao, Y. Jia, M. Zhang, J. P. Su, G. Liu, T. S. Hwang, S. T. Bailey, and D. Huang, "Optical coherence tomography angiography," Invest. Ophthalmol. Vis. Sci. **57**(9), OCT27–OCT36 (2016).
9. C. L. Chen and R. K. Wang, "Optical coherence tomography based angiography [Invited]," Biomed. Opt. Express **8**(2), 1056–1082 (2017).
10. I. Bhutto and G. Lutty, "Understanding age-related macular degeneration (AMD): relationships between the photoreceptor/retinal pigment epithelium/Bruch's membrane/choriocapillaris complex," Mol. Aspects Med. **33**(4), 295–317 (2012).
11. J. Tokayer, Y. Jia, A. H. Dhalla, and D. Huang, "Blood flow velocity quantification using split-spectrum amplitude-decorrelation angiography with optical coherence tomography," Biomed. Opt. Express **4**(10), 1909–1924 (2013).
12. J. P. Su, R. Chandwani, S. S. Gao, A. D. Pechauer, M. Zhang, J. Wang, Y. Jia, D. Huang, and G. Liu, "Calibration of optical coherence tomography angiography with a microfluidic chip," J. Biomed. Opt. **21**(8), 86015 (2016).
13. W. J. Choi, W. Qin, C. L. Chen, J. Wang, Q. Zhang, X. Yang, B. Z. Gao, and R. K. Wang, "Characterizing relationship between optical microangiography signals and capillary flow using microfluidic channels," Biomed. Opt. Express **7**(7), 2709–2728 (2016).
14. W. Choi, E. M. Moult, N. K. Waheed, M. Adhi, B. Lee, C. D. Lu, T. E. de Carlo, V. Jayaraman, P. J. Rosenfeld, J. S. Duker, and J. G. Fujimoto, "Ultrahigh-speed, swept-source optical coherence tomography angiography in nonexudative age-related macular degeneration with geographic atrophy," Ophthalmology **122**(12), 2532–2544 (2015).
15. S. B. Ploner, E. M. Moult, W. Choi, N. K. Waheed, B. Lee, E. A. Novais, E. D. Cole, B. Potsaid, L. Husvogt, J. Schottenhamml, A. Maier, P. J. Rosenfeld, J. S. Duker, J. Hornegger, and J. G. Fujimoto, "Toward quantitative optical coherence tomography angiography: visualizing blood flow speeds in ocular pathology using variable interscan time analysis," Retina **36**(12), S118–S126 (2016).
16. C. Blatter, T. Klein, B. Grajciar, T. Schmoll, W. Wieser, R. Andre, R. Huber, and R. A. Leitgeb, "Ultrahigh-speed non-invasive widefield angiography," J. Biomed. Opt. **17**(7), 070505 (2012).
17. R. Poddar, J. V. Migacz, D. M. Schwartz, J. S. Werner, and I. Gorczynska, "Challenges and advantages in wide-field optical coherence tomography angiography imaging of the human retinal and choroidal vasculature at 1.7-MHz A-scan rate," J. Biomed. Opt. **22**(10), 1–14 (2017).
18. K. V. Vienola, B. Braaf, C. K. Sheehy, Q. Yang, P. Tiruveedhula, D. W. Arathorn, J. F. de Boer, and A. Roorda, "Real-time eye motion compensation for OCT imaging with tracking SLO," Biomed. Opt. Express **3**(11), 2950–2963 (2012).
19. B. Braaf, K. V. Vienola, C. K. Sheehy, Q. Yang, K. A. Vermeer, P. Tiruveedhula, D. W. Arathorn, A. Roorda, and J. F. de Boer, "Real-time eye motion correction in phase-resolved OCT angiography with tracking SLO," Biomed. Opt. Express **4**(1), 51–65 (2013).
20. Q. Zhang, Y. Huang, T. Zhang, S. Kubach, L. An, M. Laron, U. Sharma, and R. K. Wang, "Wide-field imaging of retinal vasculature using optical coherence tomography-based microangiography provided by motion tracking," J. Biomed. Opt. **20**(6), 066008 (2015).
21. B. Braaf, K. A. Vermeer, K. V. Vienola, and J. F. de Boer, "Angiography of the retina and the choroid with phase-resolved OCT using interval-optimized backstitched B-scans," Opt. Express **20**(18), 20516–20534 (2012).
22. W. Choi, K. J. Mohler, B. Potsaid, C. D. Lu, J. J. Liu, V. Jayaraman, A. E. Cable, J. S. Duker, R. Huber, and J. G. Fujimoto, "Choriocapillaris and choroidal microvasculature imaging with ultrahigh speed OCT angiography," PLoS One **8**(12), e81499 (2013).

Biomedical Optics EXPRESS

23. J. Migacz, "Design files for UC Davis FDML OCTA system," figshare (2017) [retrieved 27 December 2017], https://doi.org/10.6084/m9.figshare.5735151.v1.
24. J. Migacz, "MATLAB script for OCTA processing," figshare (2017) [retrieved 27 December 2017], https://doi.org/10.6084/m9.figshare.5735142.v2.
25. J. Migacz, "Example dataset for OCTA processing," figshare (2017) [retrieved 27 December 2017], https://doi.org/10.6084/m9.figshare.5735154.v2.
26. R. Huber, M. Wojtkowski, and J. G. Fujimoto, "Fourier Domain Mode Locking (FDML): A new laser operating regime and applications for optical coherence tomography," Opt. Express **14**(8), 3225–3237 (2006).
27. T. Klein, W. Wieser, C. M. Eigenwillig, B. R. Biedermann, and R. Huber, "Megahertz OCT for ultrawide-field retinal imaging with a 1050 nm Fourier domain mode-locked laser," Opt. Express **19**(4), 3044–3062 (2011).
28. Y. Chen, D. M. de Bruin, C. Kerbage, and J. F. de Boer, "Spectrally balanced detection for optical frequency domain imaging," Opt. Express **15**(25), 16390–16399 (2007).
29. A. M. Rollins and J. A. Izatt, "Optimal interferometer designs for optical coherence tomography," Opt. Lett. **24**(21), 1484–1486 (1999).
30. R. Leitgeb, C. Hitzenberger, and A. Fercher, "Performance of fourier domain vs. time domain optical coherence tomography," Opt. Express **11**(8), 889–894 (2003).
31. American National Standards Institute Z136, 1, "American national standard for the safe use of lasers," Laser Institute of America, *Orlando, Florida* (2014).
32. S. Makita, Y. Hong, M. Yamanari, T. Yatagai, and Y. Yasuno, "Optical coherence angiography," Opt. Express **14**(17), 7821–7840 (2006).
33. J. Fingler, D. Schwartz, C. Yang, and S. E. Fraser, "Mobility and transverse flow visualization using phase variance contrast with spectral domain optical coherence tomography," Opt. Express **15**(20), 12636–12653 (2007).
34. D. Y. Kim, J. Fingler, J. S. Werner, D. M. Schwartz, S. E. Fraser, and R. J. Zawadzki, "In vivo volumetric imaging of human retinal circulation with phase-variance optical coherence tomography," Biomed. Opt. Express **2**(6), 1504–1513 (2011).
35. B. Braaf, K. A. Vermeer, V. A. D. P. Sicam, E. van Zeeburg, J. C. van Meurs, and J. F. de Boer, "Phase-stabilized optical frequency domain imaging at 1-µm for the measurement of blood flow in the human choroid," Opt. Express **19**(21), 20886–20903 (2011).
36. S. J. Chiu, X. T. Li, P. Nicholas, C. A. Toth, J. A. Izatt, and S. Farsiu, "Automatic segmentation of seven retinal layers in SDOCT images congruent with expert manual segmentation," Opt. Express **18**(18), 19413–19428 (2010).
37. D. T. Miller, D. R. Williams, G. M. Morris, and J. Liang, "Images of cone photoreceptors in the living human eye," Vision Res. **36**(8), 1067–1079 (1996).
38. R. F. Cooper, C. S. Langlo, A. Dubra, and J. Carroll, "Automatic detection of modal spacing (Yellott's ring) in adaptive optics scanning light ophthalmoscope images," Ophthalmic Physiol. Opt. **33**(4), 540–549 (2013).
39. K. Kurokawa, Z. Liu, and D. T. Miller, "Adaptive optics optical coherence tomography angiography for morphometric analysis of choriocapillaris [Invited]," Biomed. Opt. Express **8**(3), 1803–1822 (2017).
40. I. Gorczynska, J. V. Migacz, R. Jonnal, R. J. Zawadzki, R. Poddar, and J. S. Werner, "Imaging of the human choroid with a 1.7 MHz A-scan rate FDML swept source OCT system," Proc. SPIE 10045. Ophthalmic Technologies **XXVII**, 1004510 (2017).
41. I. Gorczynska, J. V. Migacz, R. J. Zawadzki, A. G. Capps, and J. S. Werner, "Comparison of amplitude-decorrelation, speckle-ariance and phase-variance OCT angiography methods for imaging the human retina and choroid," Biomed. Opt. Express **7**(3), 911–942 (2016).